Proceedings of HT2007
2007 ASME-JSME Thermal Engineering Summer Heat Transfer Conference
July 8-12, 2007, Vancouver, British Columbia, CANADA

HT2007-32786

NOTCH ARRANGEMENT EFFECTS ON HEAT TRANSFER IN A CHANNEL WITH CUT-FINS

Kazuya Tatsumi
Dept. of Mechanical Engineering and Science, Kyoto University, Sakyo-ku, Kyoto, 606-8501, JAPAN
tatsumi@mbox.kudpc.kyoto-u.ac.jp

Shintaro Matsuzaki
Dept. of Mechanical Engineering and Science, Kyoto University, Sakyo-ku, Kyoto, 606-8501, JAPAN
shintaro.matsuzaki@t03.mbox.media.kyoto-u.ac.jp

Kazuyoshi Nakabe
Dept. of Mechanical Engineering and Science, Kyoto University, Sakyo-ku, Kyoto, 606-8501, JAPAN
nakabe@me.kyoto-u.ac.jp

ABSTRACT

The effects of the attack-angle of the fin notch array against the main flow and size of the clearance at the fin-tip on the heat transfer and pressure loss performances of a channel with cut-fins (parallel fins with square notches) mounted on the bottom wall were evaluated in the present article. Three-dimensional numerical simulations, PIV measurements and heat transfer experiments employing a modified single-blow method were conducted to discuss these characteristics.

Larger pressure loss reduction was obtained by the cut-fins case compared with the plain-fins case (parallel fins without notches) under smaller clearance conditions, while smaller thermal resistance was achieved with larger clearance. A maximum peak, therefore, appeared in the overall performance in relation with the clearance size. Larger heat transfer coefficients were obtained with smaller attack-angles of the notch array in both experimental and numerical results, particularly under larger Reynolds number conditions. This was due to the spanwise flow generated in the area adjacent to the notch, by which renewal of the thermal boundary layer was effectively produced at the trailing edge of the notch.

INTRODUCTION

Parallel plate fins are one of the most popular techniques by means of enhancing the heat transfer area and coefficient. In the past few decades, therefore, discussion on the flow and heat transfer characteristics of fins with various kinds of shapes have been keenly discussed in developing an effective fins for compact heat exchangers and heat sinks [1-4].

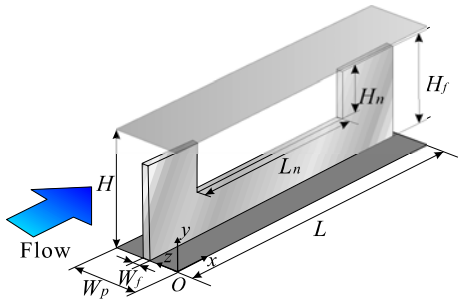

Fig. 1: Computational domain (clearance effect case).

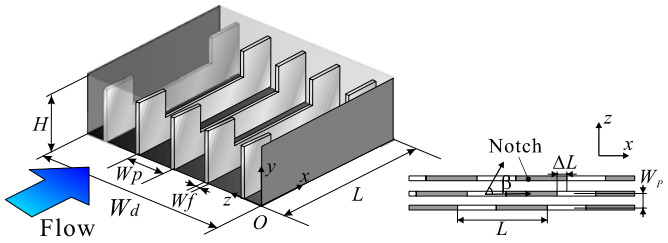

Fig. 2: Computational domain (attack-angle effect case).

When a clearance exists between the channel top wall and fin top surface, a portion of the main flow flows along this area. This affects the heat transfer performance of the fin. Namely, if the clearance is small, larger heat transfer coefficient is obtain at the fin surfaces while noticeable pressure loss penalty is incurred; on the other hand, if the clearance is large, large amount of fluid flows through the clearance that entails a

reduction of pressure loss together with deterioration of the heat transfer performance. Thus a trade-off matter between the heat transfer and pressure loss exists in relation to the clearance size [5-7].

To obtain a higher heat transfer performance in such parallel plate fins having a clearance at the fin tip, rectangular shape notches are applied to the fins (referred to as "cut-fins") in the present study. The notch is expected to convect a portion of the flow in the clearance into the area located between the fins, namely, to enhance mass and heat transfer between the fluids located at each area. This results in an increase of the heat transfer coefficient at the fin sidewalls. In addition to this, reduction of the pressure loss penalty and fin total weight are also expected as the effects of applying the notch to the fins. In the authors' previous works, the effects of the notch shape, fin spanwise pitch and notch arrangement on the flow and heat transfer characteristics of the channel have been studied by both numerical and experimental analyses [8, 9].

The advantages obtained by introducing the cut-fins to a channel, as described in the previous paragraph, are believed to be affected by the clearance size. It is important to evaluate to what extent these effects are available when the clearance size is increased. In addition to this, in the authors' previous works [8, 9], higher heat transfer performance was obtained when the notch array was set inclined to the main flow particularly in relatively high Reynolds number regime, $Re \geq 1{,}000$. This was believed to be attributed to the spanwise flow generated by the notch array, and further detail discussion should be made on the flow and heat transfer characteristics of such oblique notch array case including the effects of the attack-angle of the notch arrangement against the main flow.

Under these backgrounds, the effects of the clearance size and attack-angle of the notch array on the flow and heat transfer characteristics are examined in the present article. These characteristics are evaluated by conducting three-dimensional numerical simulations, velocity measurements using PIV (Particle Image Velocimetry) and heat transfer experiments applying modified single-blow method.

NOMENCLATURE

c : specific heat capacity
f : friction factor
h : heat transfer coefficient
H : channel height
H_f : fin height
H_n : notch height
j : Colburn j factor
L : unit length of fin
L_c : length of the test section
L_n : notch length
m : mass
Nu : Nusselt number
q : heat flux
P : pressure
Pr : Prandtl number
Re : Reynolds number
W_f : fin thickness
W_p : fin pitch
W_d : channel width

Greek symbols
β : attack-angle of notch array
λ : thermal conductivity
μ : viscosity
ρ : density
θ : temperature

Subscripts
b : bulk mean value
f : fluid part
h : harmonic mean value
inlet, *outlet*: values at inlet and outlet
m : mean value
p : plain-fin
s : solid part
w : wall

NUMERICAL PROCEDURE AND CONDITIONS

Figures 1 and 2 show the computational domain of the present numerical simulation. In Fig. 1, is shown the computational domain of the case conducted to evaluate the effects of the clearance size between the fin tip and channel top wall. In this case, periodic boundary conditions were applied to both streamwise and spanwise directions representing periodic cut-fin arrays in both directions.

The domain shown in Fig. 2 was employed in the case discussing the effects of the attack-angle against the main flow of the notch array. In the authors' previous works [8, 9], when the notch array was inclined against the main flow, spanwise flow was observed along the notch. In a channel with sidewalls, interaction between this spanwise flow and sidewalls might generate a longitudinal vortex-like secondary flow that is expected to enhance the mass and heat transfer of the fluids in the channel. To evaluate this effect, a channel with sidewalls and having 5 rows of cut-fins aligned in the spanwise direction, as shown in Fig. 2, was used as the computational domain. In this case, periodic condition was applied to the streamwise boundaries. The fin number in this case is much smaller than that of the test section used in the experiment, and relatively stronger sidewall effect will appear in the computation than in the experiment. These numerical results, however, will provide some hints to understand the flow and heat transfer characteristics of a channel with oblique cut-fins, at least in a qualitative way.

Three-dimensional incompressible and time-dependent forms of continuity and Navier-Stokes equations, as shown in Eqs. (1) and (2), were solved in the present study.

Table 1: Parameters of cut-fin array (clearance effect case).

	H/H_f	H_n/H_f	L_n/L	L/H_f	w_f/H_f	W_p/w_f
H125	1.25	0.5	0.5	4.375	0.0625	7.0
H150	1.5	0.5	0.5	4.375	0.0625	7.0
H175	1.75	0.5	0.5	4.375	0.0625	7.0
H200	2	0.5	0.5	4.375	0.0625	7.0

Table 2: Parameters of cut-fin array (attack-angle effect case).

	β [°]	H/H_f	H_n/H_f	L_n/L	L/H_f	w_f/H_f	W_p/w_f
A90	90	1.25	0.5	0.5	4.375	0.0625	7.0
A75	75	1.25	0.5	0.5	4.375	0.0625	7.0
A60	60	1.25	0.5	0.5	4.375	0.0625	7.0
A45	45	1.25	0.5	0.5	4.375	0.0625	7.0
A30	30	1.25	0.5	0.5	4.375	0.0625	7.0

$$\frac{\partial U_i}{\partial x_i} = 0 \tag{1}$$

$$\rho_f \frac{DU_i}{Dt} = -\frac{\partial P}{\partial x_i} + \frac{\partial}{\partial x_j}\left(\mu \frac{\partial U_i}{\partial x_j}\right) \tag{2}$$

Here, ρ_f and μ are the density and viscosity of the fluid, respectively.

In the computation, both temperature fields of the flow and fin were considered by solving the following energy equations of the fluid and solid parts.

$$\text{fluid part: } \rho_f \frac{D\theta}{Dt} = \frac{\partial}{\partial x_i}\left(\frac{\mu}{\Pr}\frac{\partial \theta}{\partial x_i}\right) \tag{3}$$

$$\text{solid part: } \rho_s \frac{d\theta}{dt} = \frac{\partial}{\partial x_i}\left(\frac{\lambda_s}{c_s}\frac{\partial \theta}{\partial x_i}\right) \tag{4}$$

ρ_s, λ_s and c_s are the density, thermal conductivity and specific heat capacity of the fin. At the fin surfaces, the heat flux was calculated by applying a harmonic-mean thermal conductivity defined in Eq. (5) [10].

$$q_w = -\lambda_h \frac{\partial \theta}{\partial n} \tag{5}$$

λ_h was defined as Eq. (6) using the thermal conductivities of the fluid, λ_f, and solid, λ_s.

$$\lambda_h = \frac{2}{1/\lambda_f + 1/\lambda_s} \tag{6}$$

The physical properties of air and stainless steel were applied to the fluid and solid parts under constant temperature condition. *Pr* was set equal to 0.7.

Isothermal wall condition was applied to the channel bottom wall, and the side and top walls were set as adiabatic. As mentioned above, periodic condition was applied to the streamwise boundaries. The linear pressure loss term due to the channel pressure loss in the streamwise direction was dealt by applying an additional inertia force to the source term in Eq. (2) as proposed by Patankar et al. [11]. In the thermal fields,

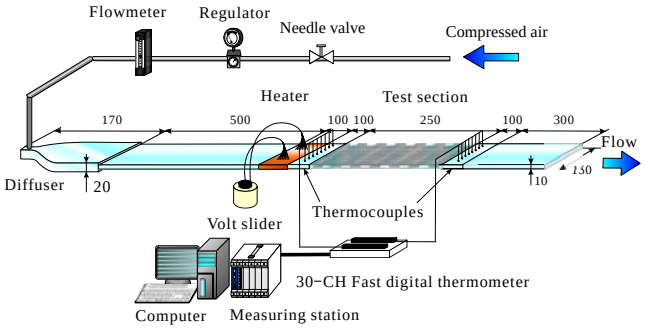

Fig. 3: Apparatus of heat transfer measurements.

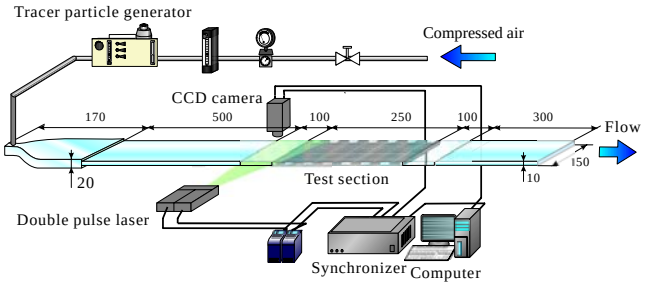

Fig. 4: Apparatus of PIV measurements.

periodic boundary conditions were applied by employing the definition that the non-dimensional temperature was equal in each periodic streamwise location as shown in Eq. (7).

$$\frac{\theta^{inlet} - \theta_w}{\theta_b^{inlet} - \theta_w} = \frac{\theta^{outlet} - \theta_w}{\theta_b^{outlet} - \theta_w} \tag{7}$$

Here θ_w and θ_b are the wall and bulk mean temperatures, respectively. The superscripts in the equation denote the locations of each boundary.

The examined parameters of the cut-fin geometry are tabulated in Tables 1 and 2. The variables shown in each table correspond to those shown in Figs. 1 and 2, respectively. In Table 1 is shown the values of the case evaluating the effects of the tip clearance. In this case, the ratio between the clearance and fin height were changed, and other variables were set constant. In the case shown in Fig. 2 and Table 2, the attack-angle of the notch array against the main flow, β, was changed from 90° to 30° by sliding each notch location in the streamwise direction with a distance of ΔL. Other geometric values, in this case, were identical with those of case H125 shown in Table 1.

Reynolds number, *Re*, was calculated on the basis of the hydraulic diameter of the channel in both cases. In the case discussing the clearance effect, *Re* was equal to 200. On the other hand, discussion on β effects was conducted under the condition of *Re*=200~2,000.

EXPERIMENTAL PROCEDURE AND CONDITIONS

In the present study, heat transfer measurement using modified single-blow method [12] and flow velocity measurement using PIV (Particle Image Velocimetry) were conducted. Figure 3 shows the apparatus of the heat transfer experiments. The air was supplied to the channel by a compressor located in the upstream. The flow rate was adjusted by a flow meter and valve that were inserted in between the channel and compressor.

In the single-blow method, the time-mean overall heat transfer coefficient was obtained by analyzing the unsteady characteristics of the flow bulk mean temperature at the inlet and outlet of the test section. When the inlet temperature is changed, the bulk temperature of the outlet flow also changes. Time histories of this outlet flow temperature depend on the inlet flow temperature, heat capacities of the fluid and fin, heat transfer area and heat transfer coefficient of the fin and channel wall. By appropriately modeling the energy equation of the test section, therefore, the heat transfer coefficients at the fin and channel walls can be predicted by finding suitable coefficients that adjust the calculated outlet temperature obtained in the computation to that obtained in the experiment.

Equations (8), (9) and (10) describe the energy equations, which model the energy balance in the test section used in the present study.

$$\frac{\partial \theta_s^*}{\partial t^*} = \theta_f^* - \theta_s^* \tag{8}$$

$$\frac{\partial \theta_w^*}{\partial t^*} = b_1\left(\theta_f^* - \theta_w^*\right) \tag{9}$$

$$\frac{\partial \theta_f^*}{\partial t^*} + \frac{\partial \theta_f^*}{\partial x^*} = b_2\left(\theta_s^* - \theta_f^*\right) + b_3\left(\theta_w^* - \theta_f^*\right) \tag{10}$$

θ^* is the dimensionless temperature defined by the initial temperature, θ^0, as $\theta^* = \left(\theta^* - \theta^0\right)/\theta^0$. t^* and x^* are the dimensionless time and distance, respectively defined as $t^* = m_s c_s t / hA$ and $x^* = hAx/\dot{m} c_f L_c$. Here m, $\dot{m}$ and L_c are the mass, mass flow rate and length of the test section, respectively. c_f is the specific heat capacity of the fluid at constant pressure. h and A are the heat transfer coefficient and heat transfer area of the fin surface. The values b_1, b_2 and b_3 are defined as follows:

$$b_1 = \frac{h_w A_w}{hA} \times \frac{m_s c_s}{m_w c_w} \tag{11}$$

$$b_2 = \frac{m_s c_s}{m_f c_f} \tag{12}$$

$$b_3 = \frac{h_w A_w}{hA} \times \frac{m_s c_s}{m_f c_f} \tag{13}$$

The subscripts *s*, *w* and *f* represent the parts of solid, channel wall and fluid, respectively.

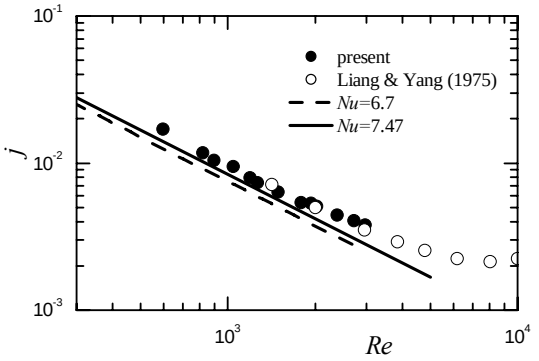

Fig. 5: Relation between *j* factor and *Re* in parallel plate case.

The partial differential equations (8), (9) and (10) were discretized by using a second order central scheme of finite difference in space and using fully implicit method in time. The obtained algebraic equations were then solved by the iteration process, to which TDMA was applied. In this case, the measured temperature of the inlet flow was applied to the inlet boundary. At the outlet boundary, the temperature gradient was set equal to zero, namely, Neumann condition was employed.

As shown in Fig. 3, an electric heater was inserted in the channel in the upstream area of the test section. This heater was consisted of a wire mesh of 0.3mm diameter weaved between the channel top and bottom wall in 10 rows. It was charged by a voltage-slider (Yamabishi V-130-3) and an electric switch under constant voltage condition, and a step-like temperature change in the inlet flow was obtained.

The flow temperatures at the inlet and outlet were measured by inserting K-type thermocouples at the inlet and outlet of the test section. Thermocouples of 0.1mm in diameter were set at each location, having 5 rows equally spaced in the spanwise direction. In each row, 3 thermocouples were inserted in equal distance in the height direction, thus, totally 15 thermocouples were applied to the inlet and outlet. The thermocouples were connected to and measured by a multi-channel thermo-meter (Yokogawa WE500, WE7232).

Considerable difference of velocity distribution from a simple Poiseuille flow pattern at the outlet was expected owing to the cut-fin arrangement, and would be a major cause of poor estimation of the bulk mean temperature. To obtain a more accurate value of the bulk mean temperature, a preliminary experiment of PIV measurements was conducted to measure the inlet and outlet velocity distributions corresponding to the positions at which the thermocouples were located.

The PIV system used in the present study was composed of a double pulsed Nd:YAG laser (New Wave Research Solo3: wave length 532nm) and a high resolution CCD camera (TSI PIVCAM 10-30: 8bit monochrome, 1Mpixels). During the PIV experiment, a particle generator (TSI model 9306) was set in the upstream of the channel, and tracing particles of oil mist (Di-Ethyl-Hexyl-Sebacate, 1.0mm in nominal diameter) were

mixed with the air. As shown in Fig. 4, a laser sheet was beamed through the channel sidewall. The CCD camera was set above of the channel, by which a pair of scattering images of the tracing particles was recorded in a certain time-difference. The velocity vectors were then calculated by using a PIV analysis software (TSI insight 3.4).

The test section was made of acrylic resin. The channel length, width and height were 250, 150 and 10mm, respectively. The fin was made of aluminum and was glued onto the channel bottom wall. The fin thickness was 0.5mm, therefore, the number of row in the spanwise direction was 42. The number of the notches in the streamwise direction was 7. The geometric parameters of the notch in the experiment were identical to those of the numerical simulation shown in Table 2. The notch attack-angle to the main flow, β, was changed under the conditions of β=90°, 75°, 60°, 45° in this case. The flow Reynolds number employed in the experiment, *Re*, was on the bases of the channel double height and mean velocity. This mean velocity was calculated from the mass flow rate measured by the flow meter located upstream of the channel. *Re* was varied from 1,000 to 2,000.

RESULTS AND DISCUSSION

Preliminary Test Case

To validate the present experimental procedure in measuring the heat transfer coefficient, a preliminary test was carried out in a parallel plate case. The test section was composed of two copper plates, which were attached to the channel top and bottom walls. The plate thickness was 0.85mm and the length of this section was 100mm. The test section was mounted to the experimental apparatus introduced in Fig. 3. The heat transfer coefficients were measured following the procedure described in the previous section.

Figure 5 shows the relation between the Colburn *j*-factor obtained from Eq. (14) and Reynolds number, *Re*. The characteristic length in calculating *Re* is the channel double height, which is the double value of the distance between the two copper plates.

$$j = St\,\mathrm{Pr}^{\frac{2}{3}} = \frac{Nu}{\mathrm{Pr}^{1/3}\,Re} \qquad (14)$$

For comparison, the results of Liang and Yang [12] are also included in the figure. The lines in the figure illustrate the values of *Nu* =6.7 and 7.47 that respectively represent the cases of parallel plates with isothermal and constant heat flux conditions. The results obtained in the present study agree very well with those of the reference, particularly under lower *Re* conditions. As *Re* increases, *j* slightly deviates from the linear line and a larger value is obtained in the present case compared with that obtained in the reference. This is believed to be attributed to the developing region of the thermal boundary layer located at the front edge of the test section. In this area, lager heat transfer coefficient is obtained that becomes large enough to affect the overall heat transfer coefficient when *Re* increases due to the insufficient streamwise length of the test section.

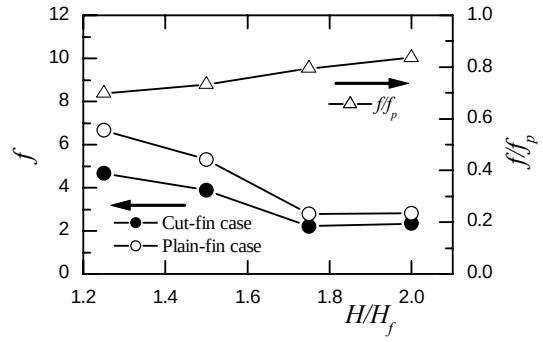

Fig. 6: Fin height to channel height ratio effects (clearance effects) on friction factor, f, (*Re*=200).

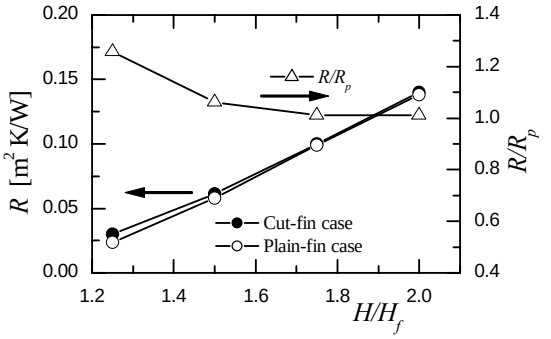

Fig. 7: Fin height to channel height ratio effects (clearance effects) on thermal resistance, *R*, (*Re*=200).

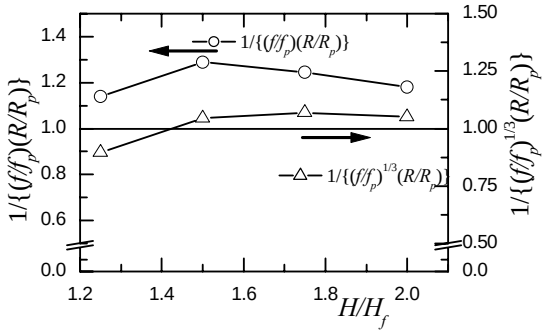

Fig. 8: Fin height to channel height ratio effects (clearance effects) on overall performance (*Re*=200).

Nevertheless, the results show that the procedures of the measurement and analysis employed in the present study are reasonable enough to discuss the heat transfer performance of the fins under the target regime of *Re*, which is 1,000≤*Re*≤2,000.

Clearance Effects

Figures 6 and 7 show the numerical results predicting how the clearance between the fin tip and channel top wall affects

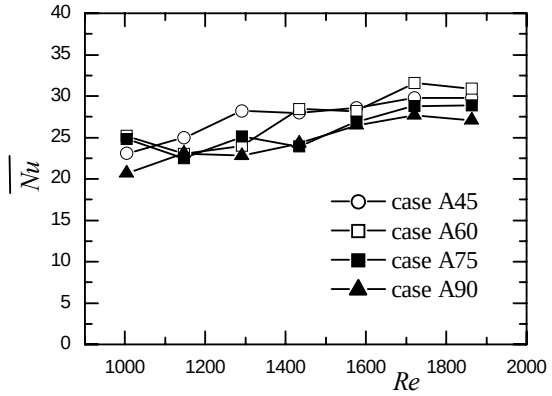

Fig. 9: Averaged Nusselt number obtained in the heat transfer experiment (attack-angle effect).

the friction factor, *f*, and thermal resistance, *R*. Reynolds number, *Re*, in this case was *Re*=200. *R* is defined as Eq. (15):

$$R = \frac{\theta_w - \theta_b^{inlet}}{q_w} \tag{15}$$

where θ_w and q_w are the wall temperature and heat flux. θ_b^{inlet} is the flow bulk mean temperature at the inlet of the computational domain. For comparison, the results of a plain-fin case, which is the case of a parallel fin array without notches, are also depicted in the figure. The values normalized by those of the plain-fin case, f_p and R_p, are also shown in the figures scaled by the right hand side axes.

As H/H_f increases, which implies an increase of the clearance, *f* decreases in both cases of cut-fin and plain-fin. This is due to the fact that the pressure loss of the flow in the clearance area becomes smaller compared with the area located between the fins. However, since this accompanies a decrease of the mass flow rate of the flow in the area between the fins, deterioration of heat transfer is incurred at the fin surfaces. This is shown in Fig. 7, where *R* increases as H/H_f increases indicating a lower heat transfer performance is obtained under larger clearance conditions.

Comparing the results obtained by the cut-fins and plain-fins, *f* is smaller in the cut-fin array case than in the plain-fin case (f/f_p is smaller than unity) under all H/H_f conditions. A reduction of the pressure loss penalty is, therefore, achieved by applying notches to parallel fins. The ratio f/f_p becomes small as H/H_f decreases, which implies that a stronger effect of the pressure loss reduction produced by the notch is obtained in the cases of smaller clearance.

On the other hand, R/R_p shown in Fig. 7 is larger than unity under all examined H/H_f conditions. Furthermore, R/R_p increases as H/H_f decreases. This indicates that the heat transfer performances in the two cases are identical or is better in the plain-fin case; and the effect of applying the notch is noticeable under larger clearance conditions.

To briefly discuss the aforementioned trade-off trends of the clearance in the overall performance of the fins, the values

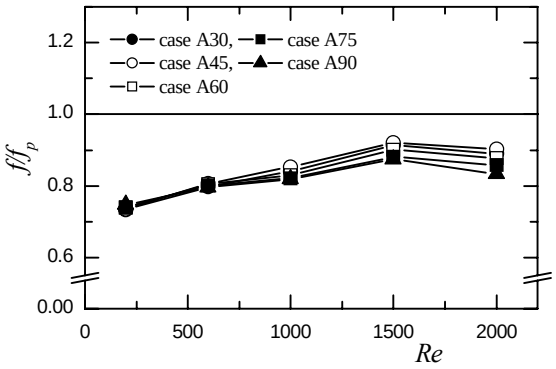

Fig. 10: Attack-angle, β, and Reynolds number, *Re*, effects on the channel friction factor, *f*.

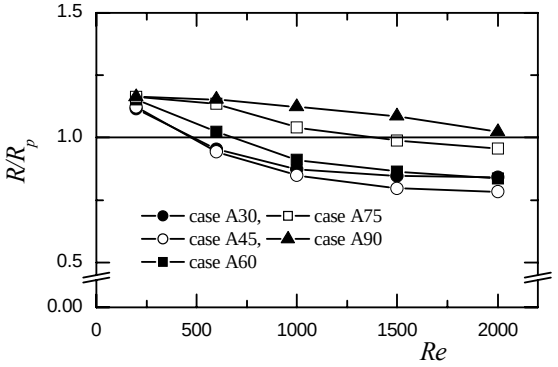

Fig. 11: Attack-angle, β, and Reynolds number, *Re*, effects on the distributions of thermal resistance, *R*.

$1/\{(f/f_p)(R/R_p)\}$ and $1/\{(f/f_p)^{1/3}(R/R_p)\}$ are shown in Fig. 8. Although these values do not precisely describe the overall performance, one can at least discuss the clearance effects in a qualitative way. Except in the case of H/H_f=1.25, both values are larger than unity and a maximum peak is observed in the area of $1.4 \le H/H_f \le 1.8$, which indicates a better performance is obtained in the cut-fin case compared with the plain-fin case.

Notch Arrangement Effects (Attack-angle effects)

Figure 9 shows the relation between the averaged Nusselt number, $\overline{Nu}$, and Reynolds number, *Re*, in the cut-fin cases obtained in the heat transfer experiment. In all attack-angle cases, $\overline{Nu}$ increases as *Re* increases, and higher heat transfer efficiency is obtained in larger *Re* regimes. The smallest $\overline{Nu}$ among the tested cases is obtained in case A90 in the present range of *Re*. Higher heat transfer coefficient is, therefore, attained by inclining the notch array. Comparing $\overline{Nu}$ of different attack-angle, β, although not clearly indicated in the

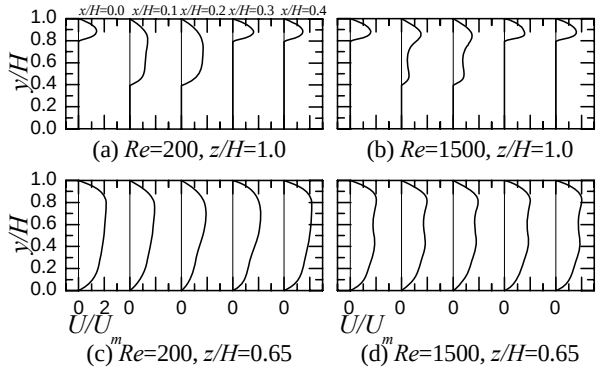

(a) *Re*=200, *z/H*=1.0 (b) *Re*=1500, *z/H*=1.0

(c) *Re*=200, *z/H*=0.65 (d) *Re*=1500, *z/H*=0.65

Fig. 12: Cross-sectional distributions of streamwise velocity, *U*, at *z/H*=0.65 and 1.0 (case A90).

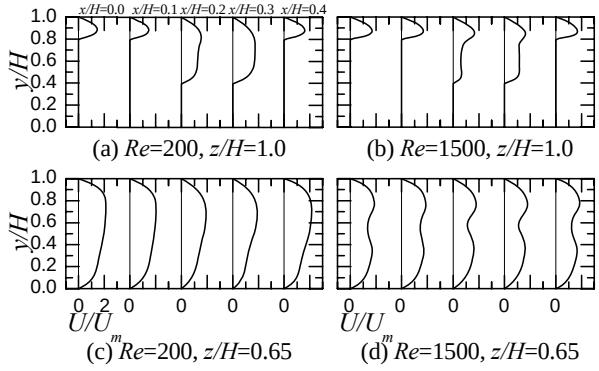

(a) *Re*=200, *z/H*=1.0 (b) *Re*=1500, *z/H*=1.0

(c) *Re*=200, *z/H*=0.65 (d) *Re*=1500, *z/H*=0.65

Fig. 13: Cross-sectional distributions of streamwise velocity, *U*, at *z/H*=0.65 and 1.0 (case A45).

figure, $\overline{Nu}$ appears to increase as β decreases, and the largest value is obtained in case A45.

Figures 10 and 11 show the numerical results of β effects on the friction factor, *f*, and thermal resistance, *R*, respectively. Both values are normalized by the results of the plain-fin case. In Fig. 10, f/f_p is smaller than unity in all cases, which implies that a reduction of pressure loss is attained in all β cases examined in the present study. f/f_p increases as *Re* increases. On the contrary, in Fig. 11, R/R_p decreases as *Re* increases implying that higher heat transfer performance is obtained particularly under the conditions of larger *Re* and smaller β. This trend is believed to be related to the secondary flow generated by inclining the notch array, which will be discussed shortly.

Figures 12 and 13 show several cross-sectional distributions of *U* at *z/H*=0.65 and 1.0 in the cases of A90 and A45. *z/H*=0.65 approximately corresponds to the middle of the area between two fins. *z/H*=1.0 is the middle of the fin located at the center of the channel. Figures 14 and 15 respectively show the streamwise velocity, *U*, contours at the cross-sectional planes of *y/H*=0.6 in cases A90 and A45. In these figures, the results obtained under the conditions of *Re*=200 and 1500 are shown, and *U* is normalized by the channel mean velocity, U_m.

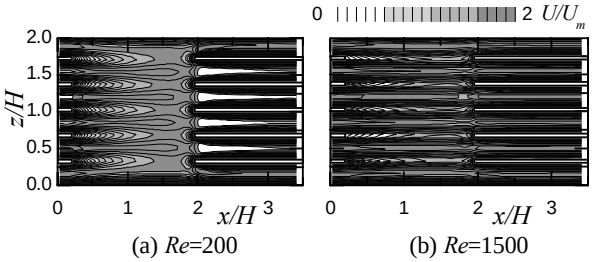

(a) *Re*=200 (b) *Re*=1500

Fig. 14: Contour maps of streamwise velocity, *U*, at *y/H*=0.6 (case A90).

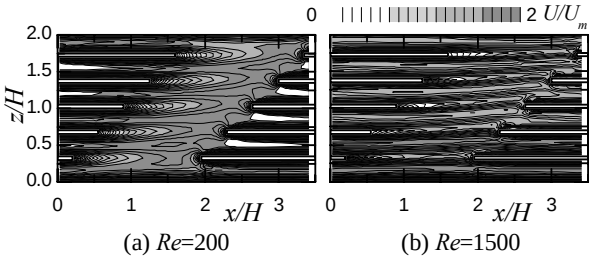

(a) *Re*=200 (b) *Re*=1500

Fig. 15: Contour maps of streamwise velocity, *U*, at *y/H*=0.6 (case A45).

In case A90 of *Re*=200 shown in Fig. 12(a) and (c), U/U_m of the flow passing between the fins decreases in the area adjacent to the notch, while U/U_m of the flow inside the notch increases. In this area, upwash flow from the lower region of the channel and downwash flow from the clearance were observed, by which the fluids in each area were brought near the fin located at the trailing side of the notch. This enhancement of the fluid mixing is one of the reasons why an equivalent heat transfer performance with the plain-fin case was obtained in this case in spite of the decrease of the heat transfer area. On the contrary, in case A90 of *Re*=1500 shown in Fig. 12(b) and (d), U/U_m distributions do not vary much in the streamwise direction. In this case, the notch effect becomes relatively small and effective upwash and downwash flows were not observed. By the notch, however, an interruption of the flow boundary layer was obtained and renewal of the thermal boundary layer was produced at the fin located in adjacent to the trailing side of the notch.

In case A45 shown in Figs. 13, a similar velocity distributions as case A90 are obtained under the condition of *Re*=200. On the other hand, in case *Re*=1500, a different flow pattern appears particularly at the location of *z/H*=0.65, i.e., two regions of large U/U_m are observed in the area near the channel top and bottom walls and a minimum peak appears near the area of *y/H*=0.5. This can also be found in comparison between Figs. 14 and 15. The U/U_m distributions in cases A90 and A45 are similar under the condition of *Re*=200. However, in case *Re*=1500, a different pattern is obtained. This difference

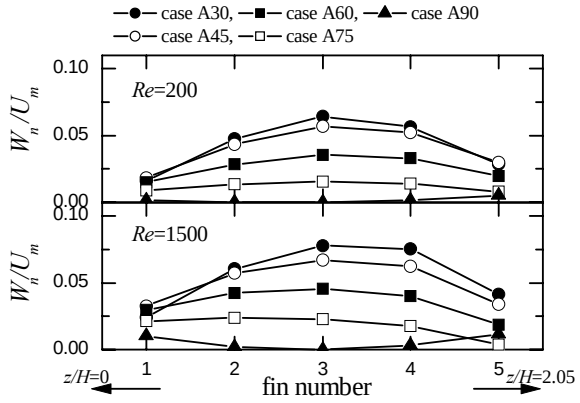

Fig. 16: Averaged spanwise velocity in the notch area, W_n.

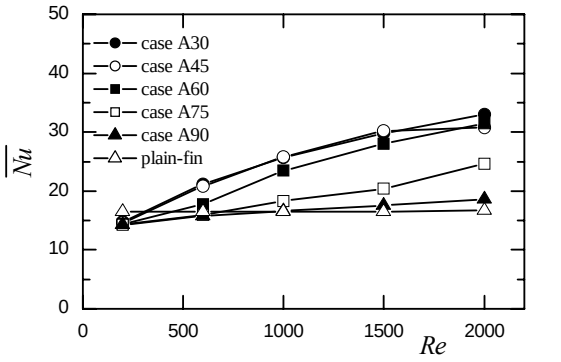

Fig. 17: Nusselt number calculated for each fin.

is considered to be owing to the spanwise flow obtained in the oblique notch array case.

Figure 16 shows the spanwise velocity averaged in the notch area obtained in cases *Re*=200 and 1500. In both cases, W_n/U_m takes a positive value indicating a spanwise flow flowing along the notch array is obtained by the inclination of the notch arrangement. W_n/U_m increases as β decreases and a maximum peak in all cases are obtained at fin number 3, which is the fin located at the channel center. Furthermore, comparing the values in cases *Re*=200 and 1500, W_n/U_m is larger in case *Re*=1500. A stronger spanwise flow is, therefore, obtained under smaller β and larger *Re* conditions.

This spanwise flow is believed to produce two significant effects that results in the enhancement of the heat transfer performance compared with case A90. One is that owing to the channel sidewalls, the spanwise flow along the notch turns its direction and flow in the reverse spanwise direction in the clearance region, resulting in a generation of a longitudinal vortex-like secondary flow. Although not large in strength, this secondary flow enhances the mixing between the fluids located at the clearance and between the fins. The other effect is that the flow passing between each fin is bent in the spanwise direction in the notch area as shown in Fig. 15(b). This produces a strong flow sweeping effect at the fin edge at the trailing side of the notch. Since stronger spanwise flow is obtained under the conditions of larger *Re* and smaller β, these effects become more conspicuous and higher heat transfer performance is obtained as discussed in Fig. 11.

Figure 17 shows the averaged Nusselt numbers, $\overline{Nu}$. Nusselt number of each fin was obtained by using its respective bulk mean temperature, θ_b^n. θ_b^n was calculated by Eq. (16), into which the temperature and velocity in the area obtained by equally dividing the cross-section into several parts were substituted.

$$\theta_b^n = \int_{A_n} \rho c_p u \theta dA \Big/ \int_{A_n} \rho c_p u dA \qquad (16)$$

Here A_n is the area with the center located in the middle of each fin (fin number *n*) and with the width and height of W_p and *H*. These definitions of Nusselt number and θ_b^n for each fin were employed here due to the fact that the heat transfer characteristics at the fin surface mainly depend on the flow passing through the fins together with the spanwise flows.

In Fig. 17, $\overline{Nu}$ of the plain-fin case is nearly constant and is unaffected by *Re*. This is due to the fact that since the distance between the two fins is small, the flow in this area is laminar flow. A fully developed thermal boundary layer of laminar flow is, therefore, obtained in this area and the heat transfer coefficient at the fin surfaces is constant to *Re*.

On the other hand, a moderate increase of $\overline{Nu}$ against *Re* is obtained in case A90. As described above, a stronger effect of the renewal of the thermal boundary layer at the trailing edge of the notch is obtained. This effect increases under larger *Re* conditions entailing larger heat transfer coefficient. In cases A30~60, $\overline{Nu}$ largely increases as *Re* increases, and $\overline{Nu}$ itself is larger compared with those obtained in cases plain-fin and A90. This is believed to be attributed to the existence of the spanwise flow as discussed in above.

CONLUSIONS

Effects of the attack-angles of notch array arrangement and the clearance size on the flow and heat transfer characteristics of a channel with cut-fins attached to the bottom wall were studied using numerical simulations, PIV measurements and heat transfer experiments employing a modified single-blow method. The major conclusions obtained in the present study are summarized in the following.

1. A maximum peak was found in the overall performance ratio between the plain-fin and cut-fin cases against the clearance size. Under smaller clearance conditions, the pressure loss penalty was largely reduced in the cut-fin case compared with the plain-fin, while a smaller thermal resistance was achieved with larger clearance. The trade-off trend between these two values produced the aforementioned maximum peak.
2. Larger overall Nusselt number was obtained in the inclined notch array cases compared with the 90° attack-angle cut-fin case, particularly under larger *Re* conditions.

3. Among the examined attack-angles, a stronger spanwise flow and maximum Nusselt number were obtained under the conditions of 30° and 45° degrees.
4. Heat transfer enhancement was obtained due to the spanwise flow generated in the notch area. The effects of this spanwise flow were considered to be twofold. One was that a longitudinal vortex like secondary flow was generated in the channel, by which the heat and mass transfer of the fluids in the area located at the clearance and between the fins were enhanced. The other was that the flow passing between the fins was bent in the spanwise direction in the region adjacent to the notch. This accompanied a stronger effect of the renewal of the thermal boundary layer at the trailing side of the notch, which entailed a higher heat transfer coefficient.
5. Averaged Nusselt number on the basis of a bulk temperature independently obtained using the flow and temperature fields around each fin, was constant to *Re* in the plain-fin. On the other hand, $\overline{Nu}$ increased as *Re* increased or attack-angle decreased, which corresponded to the results obtained by the experiment. This is due to the fact that the spanwise flow along the notch was increased in relation with *Re*.

ACKNOWLEDGMENTS

This work was financially supported by The MIKIYA Science and Technology Foundation. The authors would also like to acknowledge the Japan Aerospace Exploration Agency (JAXA) and Kyoto University Supercomputing/Large-scale computing service for providing their super-computer resources to the present numerical computations.

REFERENCES

[1] Incropera, F. P., 1988, Convection heat transfer in Electronic Equipment Cooling, ASMA J. Heat Transfer, 110, 1097-1111.

[2] Knight, R. W., Goodling, J. S. and Hall, D. J., 1991, Optimal Thermal Design of Forced Convection Heat Sinks-Analytical, ASME J. Electronic Packaging, 113, 313-321.

[3] Morega, A. M, Bejan, A. and Lee, S. W., 1995, Free Stream Cooling of a stack of parallel plates, Int. J. Heat Mass Transfer, 38, 519-531.

[4] Wirtz, R. A., Chen, W. and Zhou, R, 1994, Effect of Flow Bypass on the Performance of Longitudinal Fin Heat Sinks ASME J. Electronic Packaging, 116, 206-211.

[5] Matsubara, K., Nakabe, K. and Suzuki, K., 1996, A Three-Dimensional Numerical Study on Heat Transfer Characteristics of Flow in a Channel with Fins Attached to one Wall, Heat Transfer Science and Technology Higher Education Press, Beijing, 156-161.

[6] Min, J. Y., Jang, S. P. and Kim S. J., 2004, Effect of tip clearance on the cooling performance of a microchannel heat sink, Int. J. Heat Mass Transfer, 47, 1099-1103.

[7] Sparrow, E. M., Baliga, B. R. and Patankar, S. V., 1978, Forced Convection Heat Transfer for Shrouded Fin Array with and without Tip Clearance, ASME J. Heat Transfer, 100, 572-579.

[8] K. Tatsumi, M. Yamaguchi, Y. Nishio and K. Nakabe, 2006, Proc. of 13th Int. Heat Transfer Conference, CD-ROM (paper No. THE-15), Sydney.

[9] Tatsumi, K., Noda K. and Nakabe, K., 2005, The Effect of Cut-Fin Array Arrangement on Heat Transfer and Friction Characteristics, The 6th KSME-JSME Thermal & Fluid Engineering Conference, Korea, paper-No. EJ06.

[10] Patankar, S. V., Liu, C. H. and Sparrow, E. M., 1980, Numerical Heat Transfer and Fluid Flow, Hemisphere Publishing Corporation.

[11] Patankar, S. V., Liu, C. H. and Sparrow E. M., 1977, Fully Developed Flow and Heat Transfer in Ducts Having Streamwise-Periodic Variations of Cross-Sectional Area, ASME J. of Heat Transfer, 99, 180-186.

[12] Liang, C. Y. and Yang W-J., 1975, Modified Single-blow Technique for Performance Evaluation on Heat Transfer Surfaces, ASME J. Heat Transfer, 97, 16-21.